Marine Pollution Bulletin 193 (2023) 115117

Contents lists available at ScienceDirect

Marine Pollution Bulletin

journal homepage: www.elsevier.com/locate/marpolbul

Vertical flux of microplastic, a case study in the Southern Ocean, South Georgia

Emily Rowlands [a,b,*], Tamara Galloway [b], Matthew Cole [c], Victoria L. Peck [a], Anna Posacka [d], Sally Thorpe [a], Clara Manno [a,**]

[a] British Antarctic Survey, High Cross, Madingley Rd, Cambridge CB3 0ET, United Kingdom of Great Britain and Northern Ireland
[b] University of Exeter, Faculty of Health and Life Sciences, Streatham Campus, Stocker Rd, Exeter EX4 4PY, United Kingdom of Great Britain and Northern Ireland
[c] Plymouth marine laboratory, Prospect Pl, Plymouth PL1 3DH, United Kingdom of Great Britain and Northern Ireland
[d] Ocean Diagnostics, Suite 1102, 4464 Markham Street, Victoria, BC V8Z 7X8, Canada

ARTICLE INFO

Keywords:
Vertical transport
Fibres
Fragments
Floating sediment trap
Raman spectroscopy

ABSTRACT

Estimated plastic debris floating at the ocean surface varies depending on modelling approaches, with some suggesting unaccounted sinks for marine plastic debris due to mismatches between plastic predicted to enter the ocean and that accounted for at the surface. A major knowledge gap relates to the vertical sinking of oceanic plastic. We used an array of floating sediment traps combined with optical microscopy and Raman spectroscopy to measure the microplastic flux between 50 and 150 m water depth over 24 h within a natural harbour of the sub-Antarctic island of South Georgia. This region is influenced by fishing, tourism, and research activity. We found a 69 % decrease in microplastic flux from 50 m (306 pieces/m^2/day) to 150 m (94pieces/m^2/day). Our study confirms the occurrence of a vertical flux of microplastic in the upper water column of the Southern Ocean, which may influence zooplankton microplastic consumption and the carbon cycle.

1. Introduction

Plastics are chemically inert, persistent, and ubiquitous contaminants, posing environmental, economic and health risks (Galloway et al., 2018). If current production and waste management trends continue, roughly 12,000 Mt of plastic waste will be in landfills or the natural environment by 2050 (Geyer et al., 2017). Current estimates of plastic quantities entering our oceans are not consistent with observed concentrations in the marine environment (Cózar et al., 2014). Reasons for this discrepancy include shore deposition, incorporation within the marine food web, and fragmentation into sizes smaller than captured by common sampling techniques (sampling methods mainly measure plastics above the 300-micron range) (Andrady, 2011; Eriksen et al., 2014; van Sebille et al., 2015). One of the most influential factors for this discrepancy likely relates to a lack of data on the vertical distribution of microplastics in marine environments, with data being derived predominantly from surface trawls. Relatively few studies consider plastic concentrations within the water column, see for example Bagaev et al. (2017), Dia et al. (2018), Galgani et al. (2022)., Kanhai et al. (2018).

Oceanic plastics can fragment to form microplastics (1–1000 μm) and nanoplastics (<1 μm) (Hartmann et al., 2019) via physical processes and chemical degradation (Jiang et al., 2020) as well as being manufactured at the micro or nano scale (Alimi et al., 2017). Approximately 40 % of plastics are denser than the average seawater density (Alfaro-Núñez et al., 2021). As seawater density increases with depth, plastics with densities only marginally exceeding that of the surface seawater could sink to a depth where they achieve neutral buoyancy and remain suspended in the water column (Cózar et al., 2014). For microplastics that were initially buoyant, physical and biological drivers can cause them to sink though the water column. For example, wind driven mixing can drive buoyant microplastics down from the ocean surface (Cózar et al., 2017; Kukulka et al., 2012; Poulain et al., 2019) and, biofouling and incorporation into biological matrices (e.g., heteroaggregates, faeces, marine snow) can increase the density of microplastic particles (Cole et al., 2019; Cole et al., 2016; Porter et al., 2018). Field observations have also shown that biofouled plastic debris can undergo defouling when submerged, potentially allowing these particles to float back up to the surface; this process of biofouling-and-defouling might

* Correspondence to: E. Rowlands, British Antarctic Survey, High Cross, Madingley Rd, Cambridge CB3 0ET, United Kingdom of Great Britain and Northern Ireland.
** Corresponding author.
E-mail addresses: emirow@bas.ac.uk (E. Rowlands), clanno@bas.ac.uk (C. Manno).

https://doi.org/10.1016/j.marpolbul.2023.115117
Received 27 October 2022; Received in revised form 26 May 2023; Accepted 28 May 2023
Available online 16 June 2023

lead to cyclical transport of particles (Kooi et al., 2021; Ye and Andrady, 1991).

Marine sediment cores have been used to determine quantities of plastic reaching the sea floor, facilitating microplastic flux calculations. These data are far sparser than from water samples collected at the ocean surface (Enders et al., 2019). Additionally, uncertainties in the dating of sediment cores are large, due to error margins ranging up to tens of years (Saarni et al., 2021). Sediment traps, conventionally used to quantify seasonal sedimentation of biogeochemical particles (Ojala et al., 2013) are now beginning to be used for microplastics analyses (Saarni et al., 2021; Galgani et al., 2022; Reineccius and Waniek, 2022) and could be a valuable tool for providing further insight into microplastic fluxes (Saarni et al., 2021). Sediment traps enable the capture of sinking plastic debris over pre-selected time periods and therefore avoid temporal inaccuracies in flux calculations. Additionally, they can be positioned at different depths in the water column to enable assessment of fluxes at various depths (Saarni et al., 2021; Galgani et al., 2022) and can be fixed to moorings (Reineccius et al., 2020) or free-floating (Galgani et al., 2022). They can consequently allow for more accurate flux calculations that those provided from sediment cores, which can be aligned with the physicochemical environmental parameters at trap depths. Observing the behaviour of microplastic fibres and fragments of different buoyancies below the sea surface, which have not yet settled to the seabed, can advance our understanding of microplastic pathways in the ocean.

In the Southern Ocean, microplastic debris has been detected at the ocean surface (e.g., Jones-Williams et al., 2020; Suaria, 2020b), seafloor (e.g., Munari et al., 2017; Reed et al., 2018) and, in a range of pelagic (Cannon, 1928; Jones-Williams et al., 2020) and benthic fauna (Sfriso et al., 2020). The mountainous and glaciated sub-Antarctic island of South Georgia (54.5° S, 37° W) is located south of the Polar Front (Orsi et al., 1995) in the southwest Atlantic sector of the Southern Ocean. South Georgia represents one of the most productive ecosystems in the Southern Ocean, hosting large colonies of higher predators such as fur seals, albatrosses, penguins, and whales (Smetacek and Nicol, 2005) sustained by a high concentration of Antarctic krill (*Euphausia superba*), hereafter krill). The waters around South Georgia are among the most important regions for carbon sequestration in the world's oceans, with particularly high fluxes to the deep sea (Belcher et al., 2017; Manno et al., 2020). In the nearshore waters of South Georgia, concentrations of microplastics in the surface waters have been found to be higher than elsewhere in the Southern Ocean (Buckingham et al., 2022) including open waters and nearby to the Antarctic continent (e.g., Cincinelli et al., 2017; Isobe et al., 2017; Suaria et al., 2020a, b). King Edward Cove is an area of particularly high marine traffic since all vessels operating in South Georgia are required to visit the government office at King Edward Point. Patagonian toothfish (*Dissostichus Eleginoides*) and krill fisheries are managed within South Georgia waters, with 40 registered vessels operating year-round (Government of South Georgia and the South Sandwich Islands Annual Visitor Report July 2018 to June 2019). South Georgia is also a popular tourist destination, with over 10,000 visitors per annum (Government of South Georgia and the South Sandwich Islands Annual Visitor Report July 2018 to June 2019). King Edward Point is also home to a marine and fisheries research station, open throughout the year. Each of these human influences increase the potential for locally derived sources of anthropogenic pollution.

Using a multi-level vertical sediment trap array, this study provides new insights into the vertical flux of microplastic though the water column of King Edward Cove, South Georgia. Determining the vertical flux of microplastic through the water column is critical for understanding the distribution and abundance of oceanic plastics, as well as determining microplastic bioavailability to marine organisms and potential plastic/ecosystem interactions (Kukulka et al., 2012; Law, 2017; Reisser et al., 2015). This information can better inform modelling studies of oceanic plastics and aid implementation of effective policy and conservation strategies.

2. Methods

2.1. Sample sites and trap deployment

A vertical sediment trap array was deployed for 24 h on 19 January 2019 from *RRS Discovery* in King Edward Cove, within Cumberland East Bay which is midway along the northern coast of South Georgia (54.260°S, 36.439°W, Fig. 1).

The trap array was tethered to the starboard side of the ship whilst deployed to ensure that it remained in the bay throughout the deployment. The floating sediment trap (Fig. 2) was ~5 m from the ship. A minimum acceptance level of 2 m is acknowledged to minimise ship-based contamination (Michida et al., 2019).

The floating sediment trap array (purchased from KC Denmark A/S) is a vertical series of three stainless-steel frames, each containing four Perspex 8.5 l tubes (traps). At the top of the trap array a single small surface buoy was attached to maintain buoyancy. At the bottom, a 50 kg steel weight was added to ensure the tubes were kept in an upright position. The trap frames were placed at 50 m intervals, at depths of 50 m, 100 m and 150 m. Each trap (104 mm inner diameter, 1000 mm height) had a lid which was cocked and deployed in the open position. The trap array was equipped with a firing mechanism to close the trap lids at depth. The deployment had a 100 % success rate with all lids closing, ensuring samples accurately reflected the sampling depths and avoiding contamination during recovery.

A Conductivity-Temperature-Depth (CTD) unit (SBE 911 plus / 917 plus) equipped with a fluorometer was used to vertically profile the water column <1 km from the sampling site on 20 January 2019. This provided temperature, salinity and fluorescence data. CTD data were processed according to standard British Oceanographic Data Centre (BODC) and British Antarctic Survey (BAS) protocols, and fluorescence was converted to chlorophyll *a* using the manufacturer's calibration routine (DY098 Cruise Report Polar Ocean Ecosystem Time Series-Western Core Box, 2019). In-situ and potential density were calculated from the CTD temperature, salinity, and pressure data using the seawater toolbox of Matlab, which uses the EOS 80 polynomial (Fofonoff and Millard Jr, 1983).

2.2. On-board sample preparation

Two traps per sampling depth (50, 100, 150 m) were processed for microplastic analyses. The contents of each trap were decanted into plastic measuring jugs that had been washed three times with Milli-Q prior to use and covered with aluminium foil to minimise contamination. Samples were then filtered onto a 45 μm nylon mesh using a vacuum pump filtration set-up. During filtration, when not decanting liquid, all filtration equipment was covered with aluminium foil to prevent airborne contamination. Additionally, a wetted polycarbonate filter (diameter 47 mm, pore size 1 μm) was exposed to the air each time the aluminium foil was removed to monitor airborne contamination. After the filtration process, the nylon filters were then folded, placed in round-bottom centrifuge tubes and frozen at −20 °C.

2.3. Laboratory analysis

2.3.1. Microplastic analyses

Quantification of microplastic loads was achieved with a two-step analysis: (1) visual microscopy identification of suspect microplastics in each sample and (2) a single point Raman analysis for polymer identification of each suspected microplastic.

To prepare the samples for microscopy analysis, the filters were transferred from the 50 ml centrifuge tubes used for frozen storage onto 47 mm diameter plastic Petri dishes (PALL). This was carried out inside a laminar flow hood to control for airborne contamination. Filters were initially examined under a stereo microscope (AmScope, 2×-225× Trinocular Stereomicroscope) coupled to a camera and Image J software

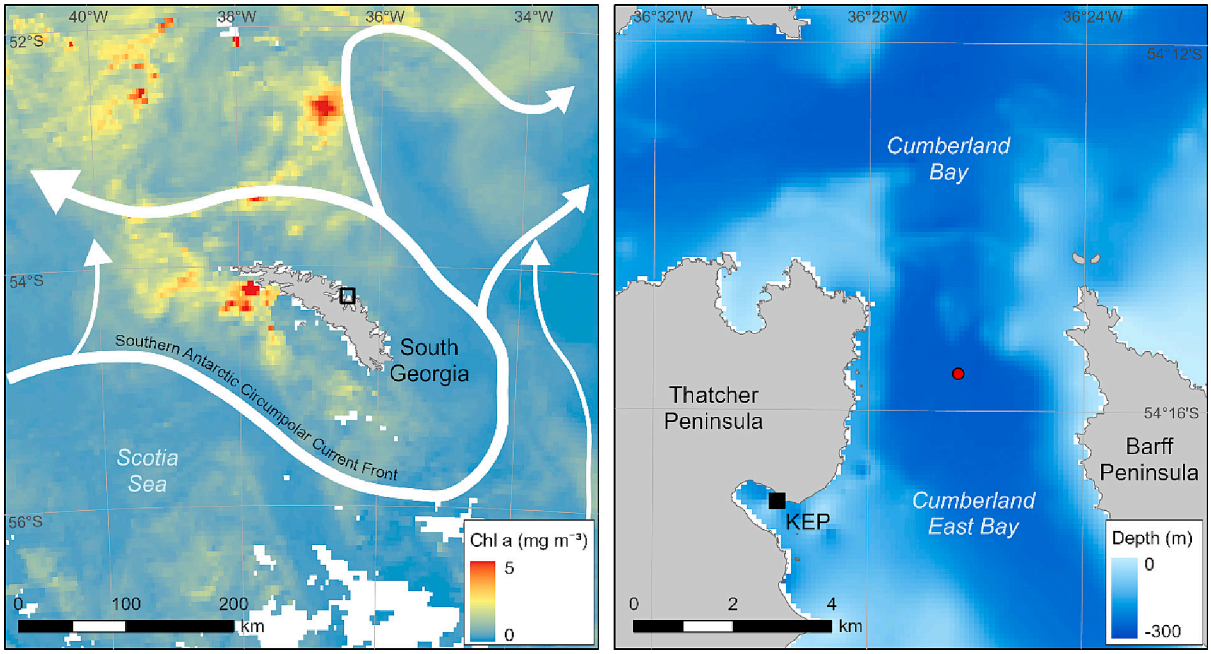

Fig. 1. (A) Sample site location at the northern coast of South Georgia. Shading indicates monthly mean chlorophyll *a* concentration (mg m^{-3}) from MODIS-Aqua for January 2019 (Goddard Space Flight Center, NASA and Ocean Ecology Laboratory, 2014) and arrows indicate the major ocean currents around South Georgia, based on Matano et al. (2020). (B) Trap array deployment location within King Edward Cove (red marker) and local bathymetry (Hogg et al., 2016). The location of King Edward Point research station is marked (KEP). (For interpretation of the references to colour in this figure legend, the reader is referred to the web version of this article.)

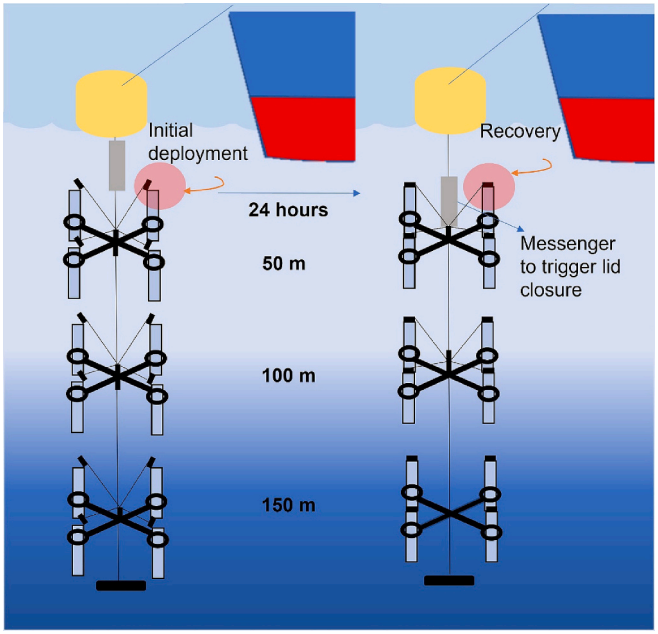

Fig. 2. A schematic of the floating sediment trap array.

to assess particle loads and distribution, with the petri dish lid closed. A relatively low matrix background enabled a good visual assessment of fibres and particles >45 μm.

To screen for and enumerate suspected microplastics, filters were divided into 5 × 5 mm areas with the help of a gridded adhesive on the petri dish lid. Plastic selection criteria were adopted based on previous recommendations (Hidalgo-Ruz et al., 2012; Lusher et al., 2020): (i) the candidate contains no visible cellular structures; (ii) the fibre has a uniform width and even coloration; (iii) the ends of the fibre are flat and not tapered to a point or frayed; and (iv) the fibre curls, crimps, or bends in three dimensions, and can stand partially upright on the filter or microscope slide. A separate set of visual criteria was adapted for non-fibrous particles that included: (i) the candidate has sharp, relatively straight edges and even colouration and (ii) the particle does not easily deform or break apart when poked with a fine needle (Hidalgo-Ruz et al., 2012; Ross et al., 2021). Candidates within each grid cell were investigated using these criteria and the location of suspect microplastics on the filter logged. This was performed with the petri dish lid closed to prevent airborne contamination. Since a mesh size of 45 μm was used, and potential microplastic candidates were identified by eye, the smallest categorised fragment range, based on the maximum ferret diameter, was 50–100 μm.

Once the visual assessment was completed, suspected microplastics from each filter were transferred onto double-sided permanent tape (Scotch® 3 M™) adhered onto gridded microscope slides. This process was performed inside a purpose-built clean area within an isolated laboratory. Each candidate was characterized in terms of its type (fragment, fibre, bead), size dimensions (ferret minimum (width) and maximum (length) for fragments, and ferret minimum (width) and longest dimension traced using ImageJ software for fibres), area, and colour. Each candidate was photographed and assigned a unique number identifier.

Each candidate was measured using an inVia™ confocal Raman microscope (Renishaw, UK) controlled by WiRE software (version 4.4.0.6908). Candidates were first visually identified and focused using a 20×/0.40 magnification objective lens (Leica, N Plan EPI) in bright field mode with the light microscope. Raman spectra were acquired with 532 nm and 785 nm lasers (RL532C50 model, Renishaw UK) as an excitation source. Raman spectra were acquired in 2–3 spots on each particle to identify the area with the highest signal-noise ratio. The inVia™ spectrometer was equipped with a diffraction grating with a density of 2400 l mm^{-1}. Centrus 08HQ36 sensor (Renishaw) was used as the detector. Before candidates were measured, the Raman spectra of a piece of silicon wafer was acquired to calibrate the instrument. All collected sample spectra as a function of the Stokes shift were centred at

1500 cm^{-1} with a range of 950 to 2000 cm^{-1}. Laser power and acquisition time were recorded for every candidate. Measured spectra were compared to reference spectra of virgin and weathered plastics from open-source libraries [OpenSpecy (Cowger et al., 2020), SLoPP and SLoPP-E (Munno et al., 2020)] using in-house software based on Pearson correlation spectral matching. In some cases, commercial libraries (KnowItAll, Willey) were used for cross-referencing of data and quality control. The Pearson correlation coefficient, r, is used directly as the Hit Quality Index (HQI). Additional information on spectral data collection and quality assurance can be found in the Supplementary Information (S1).

2.4. Anti-contamination protocol

To minimise and identify potential contamination of the samples, specific measures were put in place aboard the *RRS Discovery*. Foot traffic in and out of the lab was limited to scientists involved in sample transfer and filtration. Each scientist wore a cotton lab coat. All laboratory equipment was acid washed before deployment, cleaned with Milli-Q three times in between each sample, and covered with aluminium foil when not being used. Potential sources of contamination on the deck were identified, photographed and samples taken to be added to a specific ship deck contamination library. This included polymeric paints, polyamide rope and other kit being operated from the aft deck. Prior to deployment, all parts of the floating sediment trap and the trap bottles were flushed with filtered sea water. Lids were not cocked until the moment of deployment to minimise airborne contamination. Trap lids were triggered to close at depth prior to recovery, minimising the risk of airborne contamination whilst recovering the trap array onto the aft deck.

2.5. Data analyses

2.5.1. Mass calculations

Determining the mass of microplastic was achieved using an extended method of Simon et al. (2018) which limits the overestimation of mass by crudely accounting for (unobserved) concavity in the thickness dimension. Calculations were specific to fragments or fibres.

For fragments, volume was calculated as cross-sectional area multiplied by thickness. ImageJ area (A_{ImageJ}) measurements, which account for concave regions of the 2D shape, were multiplied by fragment thickness (T) after adjusting thickness to account for potential (unobserved) concavity across the 3rd dimension. Thickness was estimated from length and width measurements by assuming equality of the width/length and thickness/width ratios. Then, to account for concavity, an adjusted thickness was calculated as P*T, where $P = A_{ImageJ} / (L*W)$ is the proportion of the bounding rectangle filled by the 2D shape. The volume calculation was therefore: $V=P*T*A_{ImageJ}$. Fragment mass was then calculated by multiplying volume by the polymer density found in the Supplementary Information (S2).

For fibres, the mass was calculated by assuming fibres were flexible cylinders, using the feret minimum (width) and maximum (length) measurements in the following equation $V = (\pi \times W^{2} \times L) / 4$ and multiplying by the density of the identified polymer.

2.5.2. Flux calculations

Flux calculations also varied according to microplastic type. For fragments, only those confirmed as plastic were included in microplastic flux calculations. Although cleaning treatments were implemented to enhance the success of polymer identification, many fibres identified as anthropogenic (synthetic and non-synthetic) were challenging to identify to their polymer category due to degradation. To account for this, the percentage of confirmed microplastic fibres from all polymer-confirmed fibres from each depth (38.09 %, 46.94 % and 37.93 % from the top, middle and bottom depths respectively) was applied to the non-polymer confirmed fibres, to extrapolate the predicted numbers of synthetic fibres in each sample (the microplastic fluxes including only spectral matches can be found in the Supplementary Information (S3) for comparison). The relevant percentage of unidentified spectra at each depth, which were expected to be microplastic, were selected using a random number generator.

2.5.3. Statistical analyses

Statistical analyses were conducted in SPSS 28.0.1.0. Differences between fibre and fragment sizes at each trap depth were tested using ANOVA and post hoc Tukey's tests. Assumptions of normality were assessed by visual inspection of Normal Q-Q plots.

3. Results

3.1. Physicochemical environmental conditions

At the time of sampling, the upper 25 m of the water column contained a layer of fresh water, creating a relatively shallow halocline and pycnocline beneath it (Fig. 3). The halocline coincided with peaks in both potential temperature and chlorophyll *a* concentration (3.3 °C and 1.2 μg l^{-1} respectively). Beneath this, the water was well mixed to a depth of approximately 60 m, after which potential temperature decreased to 1.2 °C and salinity increased to 34.05 at 250 m. Comparison of the sediment trap depths with the potential density profile shows the first sediment trap was located below the near-surface pycnocline but within the deeper layer of well-mixed waters, and the second and third traps were in the stratified waters beneath. In-situ density at the three sediment traps ranged from 1027.2 kg m^{-3} at 50 m to 1027.8 kg m^{-3} at 150 m.

3.2. Microplastic contamination

A total of 7 fibres were identified on the aerial blank from the water filtration. Spectral analysis confirmed 2 polyester fibres (1 blue, 1 black), 1 synthetic black fibre, and four of the spectra were unidentifiable (2 orange, 1 black and 1 brown fibre). Since a percentage of the spectra were unidentifiable, a precautionary approach was adopted assuming air pollution had a random composition and therefore all 7 fibres were deemed to be microplastic for the purpose of applying a correction factor. Microplastic abundance flux calculations were therefore adjusted to deduct the average aerial contamination ($7 / 3 = 2.33$, $n = 2$ for each of the 3 depths). Mass fluxes were adjusted to remove the total mass of fibres present on the air contamination filter (which equated to 2.5 μg/m^2/day per depth) from microplastic fibre flux and total microplastic flux calculations. Mass fluxes were also adjusted to remove the blue polypropylene fibre identified at each depth (which equated to 0.8, 1.7 and 1.5 μg/m^2/day for the 50, 100 and 150 m depths respectively).

Of the 12 materials collected from the ship as potential contamination sources (polymeric paints, polyamide rope and other kit being operated from the aft deck), 7 were identified as plastics and 5 were unidentifiable. The identifiable ship materials were cross referenced with the spectra of all microplastic candidates. Only one match of colour, shape and polymer type existed, that of blue polypropylene fibres (1 at each depth of 50, 100 and 150 m). To air on the side of caution, we removed the 3 blue polypropylene fibres found in the sample from analyses. No other ship materials matched the characteristics of the recovered oceanic microplastics. For example, we collected green polypropylene and rubber fragments from possible contamination sources on deck, but the only green fragments within the samples proved to be polyethylene and polyvinyl alcohol, and we collected a white polyethylene fragment on deck, but no white fragments were found across samples. Consequently, it can be assumed that host ship contamination within samples is minimal, likely owing to the sampling method allowing containment of samples pre-recovery, unlike that of common techniques used for surface sampling.

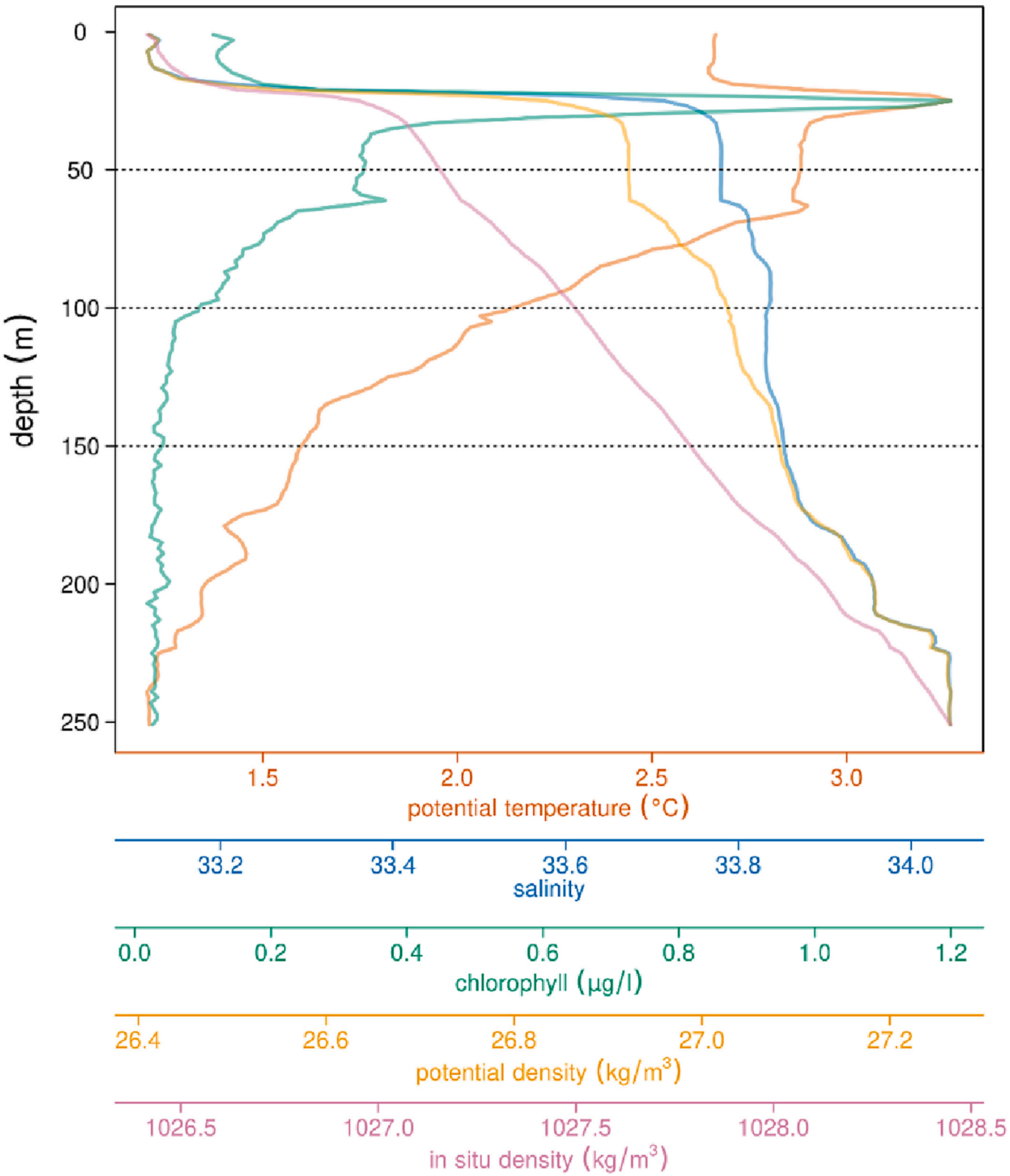

Fig. 3. Physicochemical parameters (potential temperature (°C), salinity and chlorophyll *a* (µg l^{-1}) from a Conductivity-Temperature-Depth (CTD) unit (SBE 911 plus / 917 plus) within 1 km of the sampling site with sediment trap depths (50, 100, 150 m) shown by horizontal dotted lines.

3.3. Flux of microplastics

The estimated total flux of microplastic (average of n = 2 traps per depth) decreased with depth from 306.3 pieces/m^2/day at (50 m) to 93.8 pieces/m^2/day at (150 m). The contribution of fibres to the total microplastic flux was 86 % (262.5 fibres/m^2/day) at 50 m, 97 % (212.5 fibres/m^2/day) at 100 m and 100 % (93.8 fibres/m^2/day) at 150 m. Microplastic fragment contribution to the total microplastic flux was 14 % (43.8 fragments/m^2/day) at 50 m, 3 % (6.3 fragments/m^2/day) at 100 m, and no fragments were found at 150 m. The estimated total

microplastic mass flux was highest at 100 m (1550 μg/m^2/day) with values one and two orders of magnitude lower at 50 m (158 μg/m^2/day) and 150 m (33 μg/m^2/day) respectively (Fig. 4). The contribution of fibres to the total mass flux was 97 % (152.7 μg/m^2/day) at 50 m, 22 % (342.3 μg/m^2/day) at 100 m and 100 % at 150 m. At 100 m, 78 % of the microplastic mass flux was from one large fragment.

Fibres were the dominant anthropogenic particulate recovered in our samples with optical microscopy yielding a total suspected microplastic fibre count of 118, 78 and 48 from 50, 100 and 150 m depths respectively. Spectral analyses confirmed 24 (20 %) of these fibres as microplastic from the 50 m, 23 (29 %) from 100 m and 11 (14 %) from the 150 m depth. Spectral analyses further identified 39 (33 %) fibres from the 50 m, 26 (33 %) from the 100 m and 18 (38 %) from the 150 m depth as having cellulosic properties. Whilst these candidates met the visual criteria for microplastic, the distinction between semi-synthetics and natural cellulosic fibres is not conclusive and they were eliminated from the final counts of microplastic fibres. The remaining candidates yielded unidentifiable spectra, totalling 55 (47 %) from 50 m, 29 (37 %) from 100 m and 19 (40 %) from the 150 m depth. The percentages of confirmed synthetic fibres from all identifiable fibres with a spectral match from each depth (38.09 %, 46.94 % and 37.93 % from the 50, 100, and 150 m depths respectively) was applied to the unidentified fibres to extrapolate the likely total numbers of synthetic fibres in each sample. Consequently, of 118, 78 and 48 microfibres from the 50, 100 and 150 m depth, 45, 37 and 18 fibres are deemed to be microplastic respectively. Once corrected for contamination, 42, 34, and 15 microplastic fibres were included in flux calculations from the 50, 100 and 150 m depth respectively.

Fragments were far less abundant than fibres, with a total of 14 meeting visual microplastic criteria across the three depths. Of 11 fragments from the 50 m depth optically identified, 7 were confirmed as microplastic via spectral analyses and 4 were unidentified. Of 3 optically identified fragments at 100 m, 1 was confirmed as microplastic, and 2 spectra were unidentified.

3.4. Polymer composition and characteristics

Samples collected at the 50 m depth showed the greatest variability in size of microplastic. The flux of microplastics at the smallest classified size (50–100 μm) was 6.7 % at 50 m, whilst we neglected to quantify any microplastics of this size within the 100 m and 150 m flux. Although synthetic fibres are characterized by narrow widths (10–20 μm) their lengths can vary extensively, up to several μm or even cm (Lusher et al., 2020; Ross et al., 2021; Vassilenko et al., 2021). This feature makes fibres prone to entanglement and retention on filters of various porosities, especially in samples with high particle loads. Indeed, in our samples, fibres comprised the majority of suspected microplastics, despite the use of 45 μm mesh, however short and/or thin fibres could be overlooked.

The most common microplastic size based on feret maximum was 1001–5000 μm, equating to 52.3 % of the total microplastics sampled across all depths, followed by 301–1000 μm which totalled 26.2 % across depths. The 150 m traps showed the least variability in size, with no microplastics smaller than 300 μm or >5000 μm detected (Fig. 5). The mean maximum feret diameter of microplastic significantly differed with depth (ANOVA, $F = 3.385$, $p = 0.04$). A post hoc Tukey's test showed microplastic at 100 m, which had the largest maximum feret diameter of 2670 μm ± s.e 622, was significantly larger than that at 50 m (1209 μm ± s.e 237; $p = 0.03$) but not significantly larger than at 150 m (1551 μm ± s.e 761; $p = 0.31$).

The 50 m depth displayed the greatest variability in terms of polymer type (9 polymers identified), whilst the 150 m depth showed the least variability (4 polymers). Cellulosic fibres yielded the highest abundance at each depth (52–62 %). Polyester was the most abundant synthetic fibre type with a total of 43 identified across all depths (27–32 % at each depth), followed by polypropylene with 10 fibres across all depths (4–7 % at each depth). Only 1 polyamide fibre was among the microplastic detected, found at 100 m depth and only 1 polyethylene microplastic was found, which was at 50 m depth (Fig. 7). Paints/varnishes (50 %) were the most abundant fragment type, with 4 of the 8 identified fragments being categorised as such. For microplastic fibres, blue was the most common colour (34 %), followed by transparent (30 %), black (22 %) and orange (4 %). Yellow, brown, green, pink and the mixed group were least common (2 % each). For microplastic fragments 50 % (4) were blue, 25 % (2) were green, 12.5 % (1) was orange and 12.5 % (1) silver. Diverseness in colour of fibres and fragments was highest at the 50 m depth with 7 colours identified compared to 5 at 100 m and 150 m (Fig. 6).

Three of the nine identified polymers (polypropylene, polyethylene and polystyrene) had a density lower than or equal to the in-situ seawater density, whilst six had a greater density than surrounding seawater (Fig. 7). Of positively or neutrally buoyant polymers, polypropylene was found across all depths, rubber was found at 50 m only and polystyrene at 150 m only. There was no trend of buoyant polymers being more prominent nearer the surface.

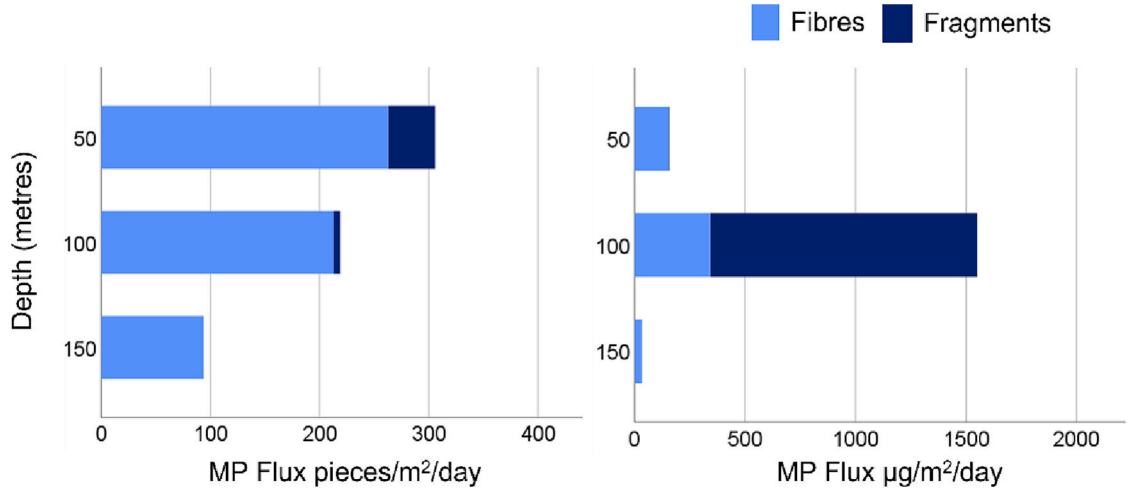

Fig. 4. Left: Total microplastic (MP) flux (pieces/m^2/day) of fibres and fragments at each measured depth. Right: Total microplastic mass flux (μg/m^2/day) of fibres and fragments at each measured depth. In both cases, light blue depicts fibres, and dark blue depicts fragments. (For interpretation of the references to colour in this figure legend, the reader is referred to the web version of this article.)

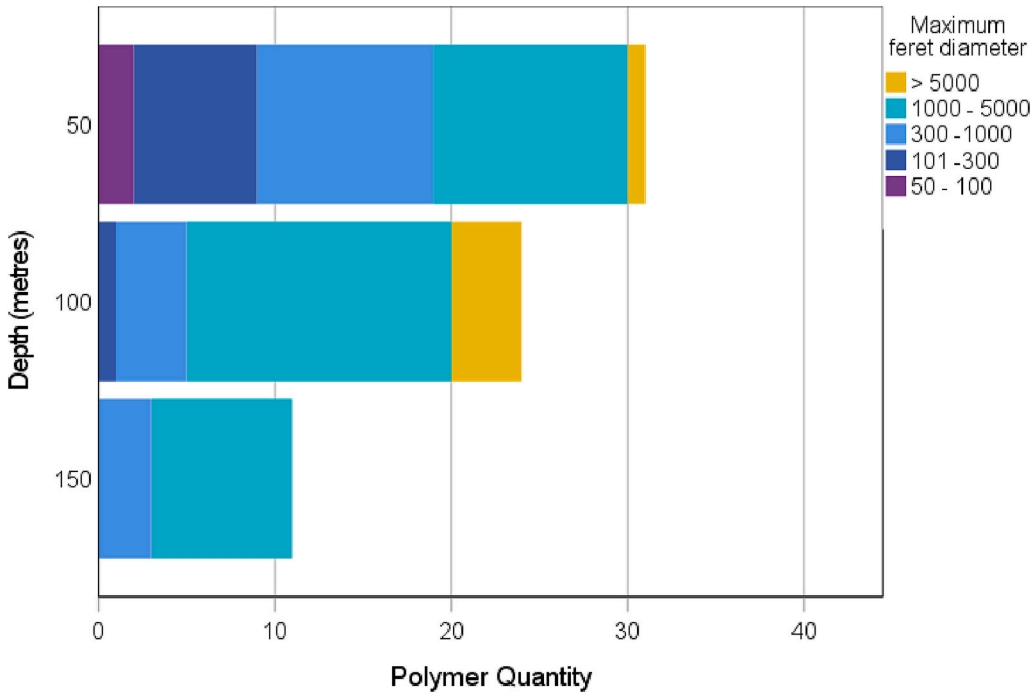

Fig. 5. Size distribution of items identified as microplastic by Raman spectroscopy based on maximum feret diameter (μm). Fibre proportions are uncorrected for contamination (n = 3 fibres per depth). Traps are grouped by deployment depth (m). N = 65 across depths (one fragment excluded due to breakage).

4. Discussion

Using a combination of a floating sediment trap array aligned with optical microscopy and Raman spectroscopy, we estimate the summer vertical flux of microplastic with a lower detection limit of 45 μm, at different depths off the northern coast of the sub-Antarctic island of South Georgia, in the Southern Ocean. We found a 69 % decrease in microplastic flux from 50 m (306 pieces/m^2/day) to 150 m (94 pieces/m^2/day). No previous studies have investigated the in-situ vertical flux of microplastic in the Southern Ocean. However, Saarni et al. (2021) estimated a summer flux of 131 pieces/m^2/day just above the sediment-water interface (water depth 11 m) of lake Haukivesi, Eastern Finland. Additionally, Reineccius et al. (2020) determined a mean microfibre flux rate (including cellulose based fibres) of 94 fibres/m^2/day in the North Atlantic Subtropical Gyre with moored sediment traps at 2000 and 3000 m. Galgani et al. (2022) with a floating sediment trap array in the North Atlantic, also calculated a microplastic mass flux between 120 μg/m^2/day (300 m) and 1700 μg/m^2/day (100 m). We calculated a microplastic mass flux in the same order of magnitude in the Southern Ocean, also finding the total microplastic mass flux was greatest at 100 m (1550 μg/m^2/day). However, the mass flux at this depth in our study was biased by one large fragment, as discussed later.

Overall, the 50 m trap contained the highest abundance of microplastic in each of the smaller size categories <1 mm. A lack of small particles reported at the ocean surface has led to the widespread statement that 99 % of microplastic smaller than 1 mm is essentially 'missing' (Cózar et al., 2014; Eriksen et al., 2014), though this has been recently debated (Weiss et al., 2021). Here we show the vertical flux of microplastic, especially in the upper 50 m of the water column, is a conduit for plastics of these smaller size categories. Our findings align with regional modelling studies e.g., Mountford and Morales Maqueda (2021) and Wichmann et al. (2019) which postulate that the majority of microplastic in the Southern Ocean will be concentrated within the top 55–60 m, below the very surface.

We also found that the dominant polymer type (polyester) at each depth was denser (1.38 g cm^{-3}) than surrounding seawater (1.03 g cm^{-3}). Whilst much less abundant, we observed positively/neutrally buoyant microplastic through to the deepest depth (polypropylene 0.95 g cm^{-3}, polystyrene 1.03 g cm^{-3}). These microplastic types may be drawn down to depths beyond their neutral buoyancy in areas of strong surface mixing and can be drawn down to depths of many hundreds of meters (Mountford and Morales Maqueda, 2021). Equally, polymers denser than seawater can be widely found in the upper water layer, e.g., Suaria et al. (2020a, b), as we go on to discuss.

Biological processes such as biofouling and zooplankton grazing could promote the flux of microplastic regardless of their density. For instance, zooplankton may incorporate microplastic in their fast-sinking faecal pellets (Bergami et al., 2020; Cole et al., 2016; Coppock et al., 2019). In-situ ingestion of microplastic in this region by krill, a key zooplankton species of the Southern Ocean ecosystem, has recently been confirmed (Wilkie Johnston et al., 2023) and the incorporation of microplastic into their faecal pellets has already been demonstrated in laboratory exposures (Bergami et al., 2020; Dawson et al., 2018). The high flux of microplastic at 50 m, just above the well mixed layer, corresponds to the preferred feeding zone for zooplankton (Ward et al., 2012).

The presence of sediment particles can also enhance the downward transport of both buoyant and negatively buoyant microplastic through the water column, due to aggregation or scavenging of microplastic by sediment. Pohl et al. (2020) exploring the role of turbidity currents in transporting microplastics concluded fibres are more homogeneously distributed throughout an artificial turbidity current compared to fragments, yet resultant deposits have an opposing trend with fibres being more abundant than fragments. They attribute this to fibres being more easily trapped between settling sediment particles than fragments. Further, Serra and Colomer (2023) show in a controlled environment that fast-settling sediment particles can scavenge slower-settling microplastics, drawing them down through the water column with scavenging being greater in calm zones compared to zones with high mixing. Differences in the vertical transport of microplastics between calm and turbulent waters is something that needs addressing further. Francalanci et al. (2021) provide a new method to predict the sinking velocity of plastic particles to further understanding of the vertical transport of microplastics in marine environments. However, they also

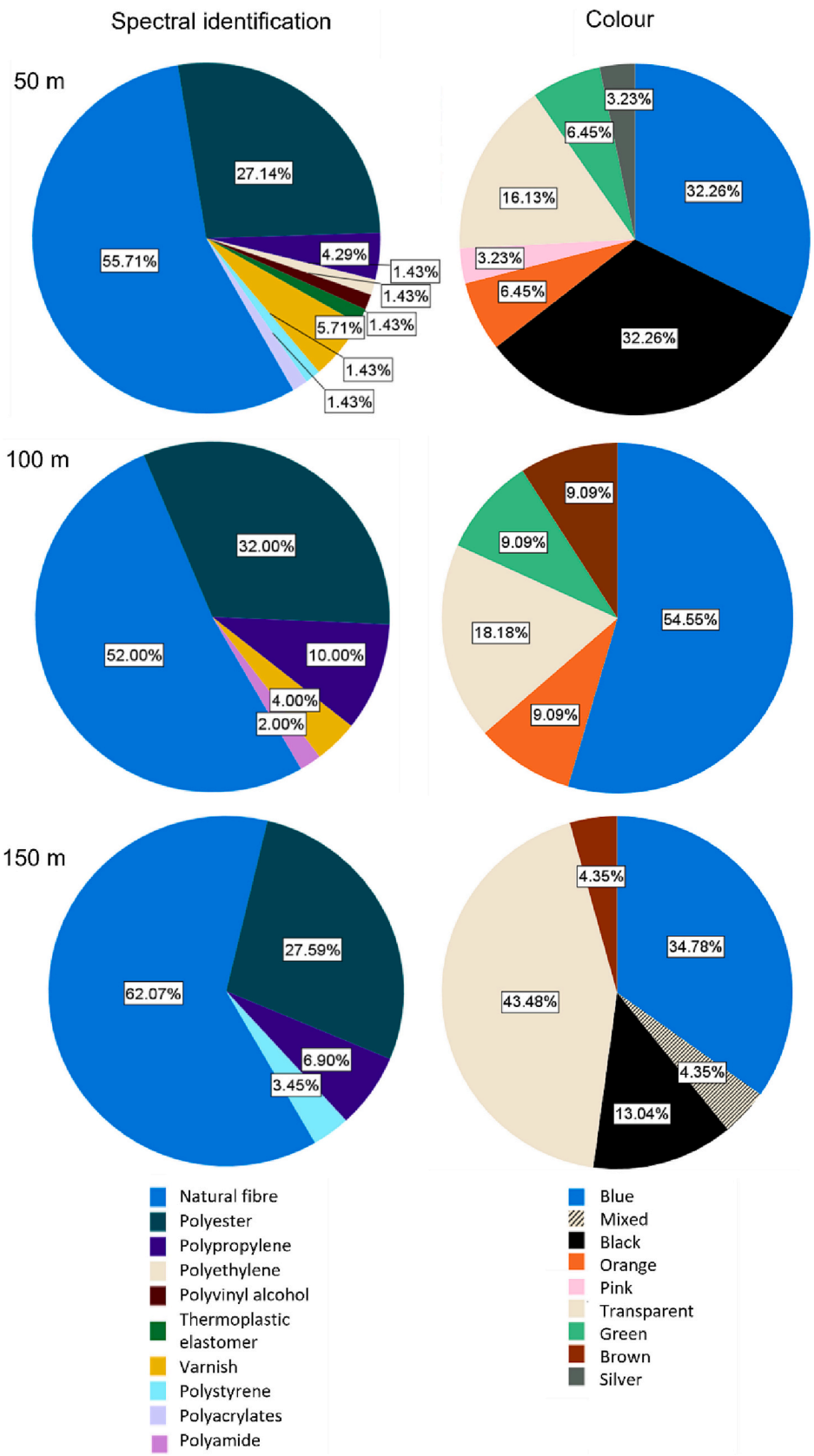

Fig. 6. Left: Total percentage of particles/fibres identified via Raman microscopy at each depth categorised by material from all identified microplastic spectra (n = 66). Right: Colour categorisation of particles and fibres identified as microplastic by Raman spectroscopy. Fibre proportions are uncorrected for contamination (n = 3 fibres per depth). (For interpretation of the references to colour in this figure legend, the reader is referred to the web version of this article.)

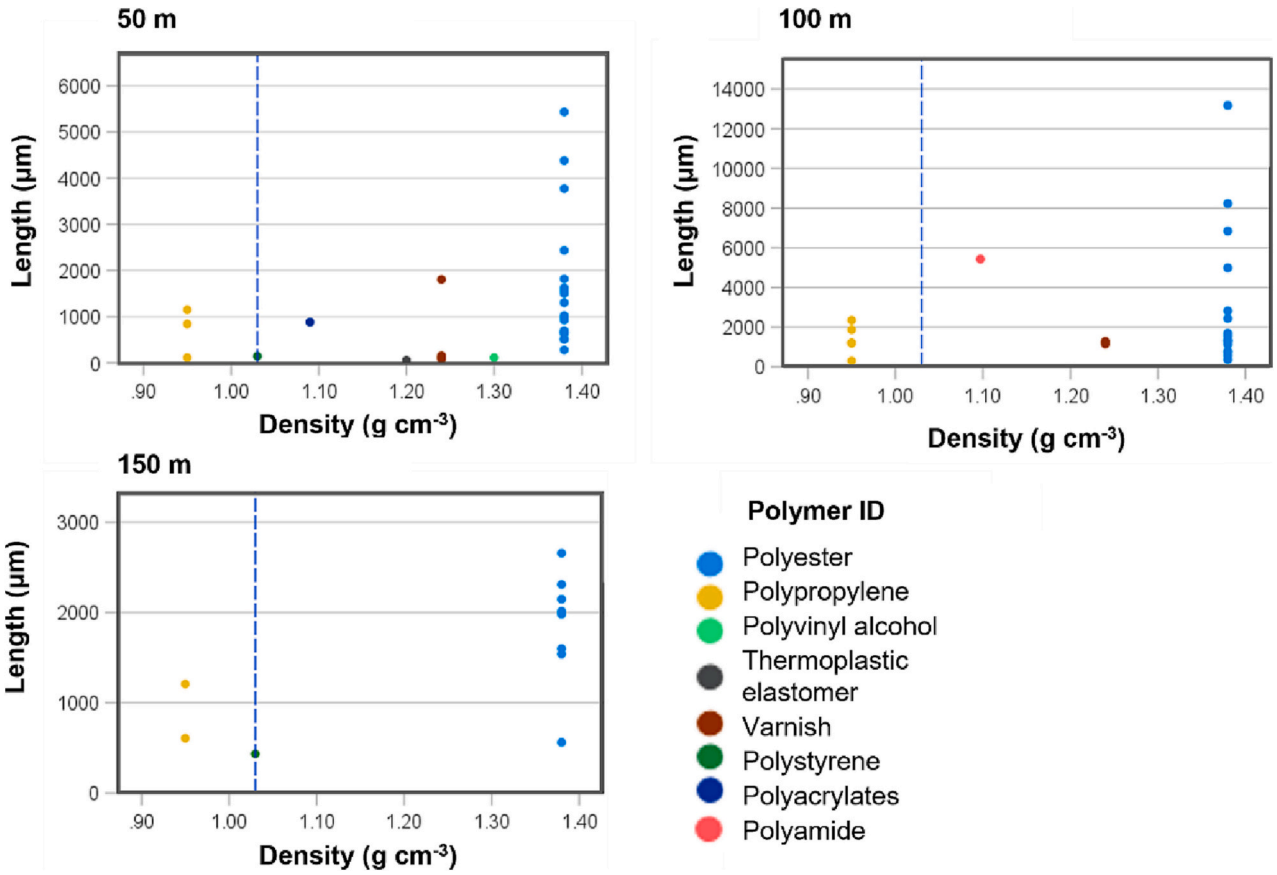

Fig. 7. Density (g cm^{-3}) of microplastic fibres and fragments at each depth (m), categorised by polymer type and size (maximum feret diameter, µm). Vertical blue line = calculated in-situ seawater density 1.03 g cm^{-3}. (For interpretation of the references to colour in this figure legend, the reader is referred to the web version of this article.)

note that the approach is currently restricted to particles in quiescent fluids and that in the case of turbulent conditions, the sinking velocity may be significantly altered. An important future step in understanding the vertical transport of microplastics in the Southern Ocean will be to account for the turbulent conditions in a more complex transport model.

Fibres dominated the microplastic flux at each depth (92 % of total microplastic) in our study. The attributes of fibres i.e., small gravitational mass, linear shape and high flexibility, means fibres readily respond to movements in their surrounding medium (Bagaev et al., 2017; Chubarenko et al., 2018). Consequently, the hydrodynamics of fibre motion can be more complicated than for fragments, and fibres are particularly susceptible to environmental influences that can keep them suspended in the water column. For example, Khatmullina and Chubarenko (2021) demonstrated that convective mixing in a laboratory environment altered the sinking behaviour of negatively buoyant fibres, with their motions becoming unsteady, leading to a reduced downward flux. The reduction in downward flux was attributed to fibres following circular motions of a convective cell. Fibres caught in a cyclic transport mechanism would align with our results of a decreasing flux at depth.

In the nearshore surface waters of South Georgia (King Edward Cove), Buckingham et al. (2022) determined that fibres accounted for 49.2 % of microplastic while Cunningham et al. (2020) found fibres contribute to 39 % of microplastic from deep sea sediment cores in three Antarctic regions including the bays and continental shelves of South Georgia, South Sandwich Islands and the Antarctic Peninsula. Whilst different environments, collection methods and analytic techniques must be considered, our findings indicate that the proportion of fibres versus fragments flux in the water column (92 % fibres) differs to the concentration at the sea surface and within marine oceanic sediments, highlighting once again the presence of different biotic and abiotic driver mechanisms.

Buckingham et al. (2022) calculated the potential annual release of microfibres from ships and stations within Cumberland Bay, South Georgia to be between 8.6 and 36.8 million. However, it should be noted that ships are prohibited from expelling grey water (domestic waste, including laundry effluence) into the marine environment within 12 nautical miles of the South Georgia coast. We found polyester was the most abundant polymer of our microplastic fibres. From sediment cores in the region, Cunningham et al. (2020) also found polyester, commonly used in the fishing industry, to be the most abundant microplastic fibre polymers. For fragments, paint/varnish dominated the identifiable polymers (50 %) reflecting the widespread application of polymer-based varnish for protective coatings of surfaces, including ships (Lacerda et al., 2019). Other studies in the Southern Ocean also highlight the emergence of a new subset of paint polymers from antifouling paint (e.g., Lacerda et al. (2019); Suaria et al. (2020b)). This raises cause for concern due to the presence of toxic additives to the antifouling paint such as metals and booster biocides used to prevent the growth of organisms (Soroldoni et al., 2017).

The sampling location of King Edward Cove, within Cumberland Bay, is subject to a relatively high level of vessel traffic with 105 vessels visiting during the same year in which sampling for this study took place. This includes passenger and research ships, private yachts as well as fishing vessels (Government of South Georgia and the South Sandwich Islands Annual Visitor Report July 2018 to June 2019), all of which can contribute to local microplastic sources. Most vessels visit the region during the austral summer, coinciding with sampling period. Relatively little is known about the small-scale currents around South Georgia, and therefore retention in the bay is unknown. However, local inputs of microplastics in this relatively enclosed bay (with potentially slow

turnover relative to the open ocean) may be substantially higher than in the open ocean where local sources have previously been deemed too low to account for the level of microplastic pollution detected (Waller et al., 2017).

To understand the fate of microplastic in the ocean and work towards a global microplastic budget, it is suggested that quantitative microplastic flux data (g/m^2/year) are required across a range of environments (Harris, 2020). Here we show that although the abundance of microplastic flux decreased with depth when considered as pieces/m^2/day, the total microplastic mass flux was greatest at 100 m (1550 μg/m^2/day), two orders of magnitude higher than at 150 m. Our findings also highlight the importance of providing both abundance and mass data, since microplastic mass flux can be easily skewed by just a small number of large microplastics. For example, just one fragment within the 100 m trap increased the total microplastic mass flux by 78 %. To advance our understanding of the vertical flux of microplastic in the Southern Ocean, a combination of multiple short term floating sediment traps deployed across multiple seasons, and long-term moored sediment traps at both near shore and open ocean locations, pre-selected based on environmental properties (e.g., currents, sea ice) and anthropogenic activities (e.g., shipping lanes, proximity to research search stations), is required.

Funding

ER was funded by a NERC GW4+ scholarship NE/L002434/1. CM was supported by UKRI-FLF project CUPIDO (MR/T020962/1). ST was supported by National Capability-ALI funding to the Ecosystems team at the British Antarctic Survey. Work was carried out as part of the Ecosystems programme at the British Antarctic Survey and the Scotia Sea Open Ocean Laboratories (SCOOBIES) sustained observation programme at the British Antarctic Survey in the frame of a WCB-POETS survey cruise.

CRediT authorship contribution statement

Emily Rowlands – Conceptualization, Methodology, Fieldwork, Data Analysis and Original drafting of the manuscript. Tamara Galloway - General Overview, Writing - Reviewing and Editing. Matthew Cole – Data Interpretation, Writing- Reviewing and Editing. Victoria L Peck – General Overview, Writing- Reviewing and Editing. Anna Posacka – Methodology, Formal Analysis, Writing – Reviewing and Editing. Sally Thorpe, Data interpretation, Writing- Reviewing and Editing. Clara Manno - Funding acquisition, Conceptualization, Methodology, Fieldwork, Writing - Reviewing and Editing.

Declaration of competing interest

The authors declare that they have no known competing financial interests or personal relationships that could have appeared to influence the work reported in this paper.

Data availability

Data will be made available on request.

Acknowledgements

We would like to thank the staff and crew of the Discovery DY098 expedition, in particular Dean Cheeseman and Andy Leadbeater for assistance with trap deployment. We would also like to thank the British Antarctic Survey Science Support team, including Bjørg Apeland and Daniel Scott for overseeing trap deployment and functioning. For laboratory support at the British Antarctic Survey laboratory, we thank Dr. Gabi Stowasser. For optical microscopy and Raman spectroscopy analyses and raw data processing, we thank Iselle Flores and Dr. Sean Yang at Ocean Diagnostics Inc. For assistance with mass calculations and creating the plot of CTD data (Fig. 3) we thank Dr. Aidan Hunter.

Appendix A. Supplementary data

Supplementary data to this article can be found online at https://doi.org/10.1016/j.marpolbul.2023.115117.

References

Alfaro-Núñez, A., Astorga, D., Cáceres-Farías, L., Bastidas, L., Soto Villegas, C., Macay, K., Christensen, J.H., 2021. Microplastic pollution in seawater and marine organisms across the Tropical Eastern Pacific and Galápagos. Sci. Rep. 11 (1), 1–8. https://doi.org/10.1038/s41598-021-85939-3.

Alimi, O.S., Farner Budarz, J., Hernandez, L.M., Tufenkji, N., 2017. Microplastics and nanoplastics in aquatic environments: aggregation, deposition, and enhanced contaminant transport. Environ. Sci. Technol. 52, 1704–1724. https://doi.org/10.1021/acs.est.7b05559.

Andrady, A.L., 2011. Microplastics in the marine environment. Mar. Pollut. Bull. 62, 1596–1605. https://doi.org/10.1016/j.marpolbul.2011.05.030.

Bagaev, A., Mizyuk, A., Khatmullina, L., Isachenko, I., Chubarenko, I., 2017. Anthropogenic fibres in the Baltic Sea water column: field data, laboratory and numerical testing of their motion. Sci. Total Environ. 599–600, 560–571. https://doi.org/10.1016/J.SCITOTENV.2017.04.185.

Belcher, A., Manno, C., Ward, P., Henson, S.A., Sanders, R., Tarling, G.A., 2017. Copepod faecal pellet transfer through the meso- and bathypelagic layers in the Southern Ocean in spring. Biogeosciences 14, 1511–1525. https://doi.org/10.5194/bg-14-1511-2017.

Bergami, E., Manno, C., Cappello, S., Vannuccini, M.L., Corsi, I., 2020. Nanoplastics affect moulting and faecal pellet sinking in Antarctic krill (Euphausia superba) juveniles. Environ. Int. 143, 105999 https://doi.org/10.1016/j.envint.2020.105999.

Buckingham, J.W., Manno, C., Waluda, C.M., Waller, C.L., 2022. A record of microplastic in the marine nearshore waters of South Georgia. Environ. Pollut. 306, 119379 https://doi.org/10.1016/J.ENVPOL.2022.119379.

Cannon, H.G., 1928. On the feeding mechanism of the copepods, calanus finmarchicus and diaptomus gracilis. J. Exp. Biol. 6, 131–144.

Chubarenko, I., Esiukova, E., Bagaev, A., Isachenko, I., Demchenko, N., Zobkov, M., Efimova, I., Bagaeva, M., Khatmullina, L., 2018. Behavior of Microplastics in Coastal Zones. Microplastic Contamination in Aquatic Environments: An Emerging Matter of Environmental Urgency, pp. 175–223. https://doi.org/10.1016/B978-0-12-813747-5.00006-0.

Cincinelli, A., Scopetani, C., Chelazzi, D., Lombardini, E., Martellini, T., Katsoyiannis, A., Fossi, M.C., Corsolini, S., 2017. Microplastic in the surface waters of the Ross Sea (Antarctica): occurrence, distribution and characterization by FTIR. Chemosphere 175, 391–400. https://doi.org/10.1016/J.CHEMOSPHERE.2017.02.024.

Cole, M., Lindeque, P.K., Fileman, E., Clark, J., Lewis, C., Halsband, C., Galloway, T.S., 2016. Microplastics alter the properties and sinking rates of zooplankton faecal pellets. Environ. Sci. Technol. 50, 3239–3246. https://doi.org/10.1021/acs.est.5b05905.

Cole, M., Coppock, R., Lindeque, P.K., Altin, D., Reed, S., Pond, D.W., Sørensen, L., Galloway, T.S., Booth, A.M., 2019. Effects of nylon microplastic on feeding, lipid accumulation, and moulting in a coldwater copepod. Environ. Sci. Technol. 53, 7075–7082. https://doi.org/10.1021/acs.est.9b01853.

Coppock, R.L., Galloway, T.S., Cole, M., Fileman, E.S., Queirós, A.M., Lindeque, P.K., 2019. Microplastics alter feeding selectivity and faecal density in the copepod, Calanus helgolandicus. Sci. Total Environ. 687, 780–789. https://doi.org/10.1016/j.scitotenv.2019.06.009.

Cowger, W., Gray, A., Christiansen, S.H., DeFrond, H., Deshpande, A.D., Hemabessiere, L., Lee, E., Mill, L., Munno, K., Ossmann, B.E., Pittroff, M., Rochman, C., Sarau, G., Tarby, S., Primpke, S., 2020. Critical review of processing and classification techniques for Images and spectra in microplastic research. Appl. Spectrosc. 74, 989–1010. https://doi.org/10.1177/0003702820929064/FORMAT/EPUB.

Cózar, A., Echevarría, F., González-Gordillo, J.I., Irigoien, X., Úbeda, B., Hernández-León, S., Palma, Á.T., Navarro, S., García-de-Lomas, J., Ruiz, A., Fernández-de-Puelles, M.L., Duarte, C.M., 2014. Plastic debris in the open ocean. Proc. Natl. Acad. Sci. U. S. A. 111, 10239–10244. https://doi.org/10.1073/PNAS.1314705111/SUPPL_FILE/PNAS.1314705111.SAPP.PDF.

Cózar, A., Martí, E., Duarte, C.M., García-de-Lomas, J., van Sebille, E., Ballatore, T.J., Eguíluz, V.M., González-Gordillo, J.I., Pedrotti, M.L., Echevarría, F., Troublè, R., Irigoien, X., González-Gordillo, Ignacio, 2017. The Arctic Ocean as a dead end for floating plastics in the North Atlantic branch of the thermohaline circulation. Sci. Adv. 3, e1600582 https://doi.org/10.1126/sciadv.1600582.

Cunningham, E.M., Ehlers, S.M., Dick, J.T.A., Sigwart, J.D., Linse, K., Dick, J.J., Kiriakoulakis, K., 2020. High abundances of microplastic pollution in deep-sea sediments: evidence from Antarctica and the Southern Ocean. Environ. Sci. Technol. 54, 13661–13671. https://doi.org/10.1021/acs.est.0c03441.

Dawson, A.L., Kawaguchi, S., King, C.K., Townsend, K.A., King, R., Huston, W.M., Bengtson Nash, S.M., 2018. Turning microplastics into nanoplastics through digestive fragmentation by Antarctic krill. Nat. Commun. 9, 1001. https://doi.org/10.1038/s41467-018-03465-9.

Dia, Z., Zhang, H., Zhou, Q., Tian, Y., Chen, T., Tu, C., Fu, C., Luo, Y., 2018. Occurrence of microplastics in the water column and sediment in an inland sea affected by

intensive anthropogenic activities. Environ. Pollut. 242, 1557–1565. https://doi.org/10.1016/j.envpol.2018.07.131.
Ye, S., Andrady, A.L., 1991. Fouling of floating plastic debris under Biscayne Bay exposure conditions. Mar. Pollut. Bull. 22, 608–613.
DY098 Cruise Report Polar Ocean Ecosystem Time Series-Western Core Box, 2019.
Enders, K., Käppler, A., Biniasch, O., Feldens, P., Stollberg, N., Lange, X., Fischer, D., Eichhorn, K.J., Pollehne, F., Oberbeckmann, S., Labrenz, M., 2019. Tracing microplastics in aquatic environments based on sediment analogies. Sci. Rep. 9 (1), 1–15. https://doi.org/10.1038/s41598-019-50508-2.
Eriksen, M., Lebreton, L.C.M., Carson, H.S., Thiel, M., Moore, C.J., Borerro, J.C., Galgani, F., Ryan, P.G., Reisser, J., 2014. Plastic pollution in the world's oceans: more than 5 trillion plastic pieces weighing over 250,000 tons afloat at sea. PLoS One 9, 1–15. https://doi.org/10.1371/journal.pone.0111913.
Fofonoff, N.P., Millard Jr., R.C., 1983. Algorithms for the Computation of Fundamental Properties of Seawater. UNESCO, Paris, France. https://doi.org/10.25607/OBP-1450 (53pp., UNESCO Technical Papers in Marine Sciences; 44).
Francalanci, S., Paris, E., Solari, L., 2021. On the prediction of settling velocity for plastic particles of different shapes. Environ. Pollut. 290, 118068 https://doi.org/10.1016/j.envpol.2021.118068.
Galgani, L., Goßmann, I., Scholz-Bottcher, B., Jiang, X., Liu, Z., Scheidemann, L., Schlundt, C., Engel, A., 2022. Hitchhiking into the deep: how microplastic particles are exported through the biological carbon pump in the North Atlantic Ocean. Environ. Sci. Technol. 56, 15638–15649. https://doi.org/10.1021/acs.est.2c04712.
Galloway, T.S., Cole, M., Lewis, C., 2018. ORE Open Research Exeter A NOTE ON VERSIONS Interactions of microplastic debris throughout the marine ecosystem, 1, 2. https://doi.org/10.1016/j.scitotenv.2006.07.022.
Geyer, R., Jambeck, J.R., Law, K.L., 2017. Production, use, and fate of all plastics ever made. Sci. Adv. 3, 25–29. https://doi.org/10.1126/sciadv.1700782.
Goddard Space Flight Center, NASA, Ocean Ecology Laboratory, 2014. Ocean Biology Processing Group. In: MODIS-Aqua Ocean Color Data. NASA Goddard Space Flight Center, Ocean Ecology Laboratory, Ocean Biology Processing Group. https://doi.org/10.5067/AQUA/MODIS_OC.2014.0.
Government of South Georgia and the South Sandwich Islands Annual Visitor Report July 2018 to June 2019. Available at. https://www.gov.gs/docsarchive/GSGSSI/Tourism/Annual%20Visitor%20Report%202018-2019.pdf.
Harris, P.T., 2020. The fate of microplastic in marine sedimentary environments: a review and synthesis. Mar. Pollut. Bull. 158, 111398 https://doi.org/10.1016/j.marpolbul.2020.111398.
Hartmann, N.B., Hüffer, T., Thompson, R.C., Hassellöv, M., Verschoor, A., Daugaard, A. E., Rist, S., Karlsson, T., Brennholt, N., Cole, M., Herrling, M.P., Hess, M.C., Ivleva, N. P., Lusher, A.L., Wagner, M., 2019. Are we speaking the same language? Recommendations for a definition and categorization framework for plastic debris. Environ. Sci. Technol. 53, 1039–1047. https://doi.org/10.1021/acs.est.8b05297.
Hidalgo-Ruz, V., Gutow, L., Thompson, R.C., Thiel, M., 2012. Microplastics in the marine environment: a review of the methods used for identification and quantification. Environ. Sci. Technol. 46, 3060–3075. https://doi.org/10.1021/ES2031505/ASSET/IMAGES/MEDIUM/ES-2011-031505_0006.GIF.
Hogg, O.T., Huvenne, V.A., Griffiths, H.J., Dorschel, B., Linse, K., 2016. A Bathymetric Compilation of South Georgia, 1985-2015. Polar Data Centre, British Antarctic Survey, NERC, Cambridge, UK. https://doi.org/10.5285/ce8bf6be-4b5f-454c-9165-73ab4c3baf23.
Isobe, A., Uchiyama-Matsumoto, K., Uchida, K., Tokai, T., 2017. Microplastics in the Southern Ocean. Mar. Pollut. Bull. https://doi.org/10.1016/j.marpolbul.2016.09.037.
Jiang, Y., Yang, F., Zhao, Y., Wang, J., 2020. Greenland Sea Gyre increases microplastic pollution in the surface waters of the Nordic Seas. Sci. Total Environ. 712, 136484 https://doi.org/10.1016/j.scitotenv.2019.136484.
Jones-Williams, K., Galloway, T., Cole, M., Stowasser, G., Waluda, C., Manno, C., 2020. Close encounters - microplastic availability to pelagic amphipods in sub-antarctic and antarctic surface waters. Environ. Int. 140, 105792 https://doi.org/10.1016/j.envint.2020.105792.
Kanhai, L.D.K., Gårdfeldt, K., Lyashevska, O., Hassellöv, M., Thompson, R.C., O'Connor, I., 2018. Microplastics in sub-surface waters of the Arctic Central Basin. Mar. Pollut. Bull. 130, 8–18. https://doi.org/10.1016/J.MARPOLBUL.2018.03.011.
Khatmullina, L., Chubarenko, I., 2021. Thin synthetic fibers sinking in still and convectively mixing water: laboratory experiments and projection to oceanic environment. Environ. Pollut. 288, 117714 https://doi.org/10.1016/j.envpol.2021.117714.
Kooi, M., Primpke, S., Mintenig, S.M., Lorenz, C., Gerdts, G., Koelmans, A.A., 2021. Characterizing the multidimensionality of microplastics across environmental compartments. Water Res. 202, 117429. https://doi.org/10.1016/J.WATRES.2021.117429.
Kukulka, T., Proskurowski, G., Morét-Ferguson, S., Meyer, D.W., Law, K.L., 2012. The effect of wind mixing on the vertical distribution of buoyant plastic debris. Geophys. Res. Lett. 39, n/a–n/a. https://doi.org/10.1029/2012GL051116.
Lacerda, A.L.d.F, Rodrigues, L. dos S., van Sebille, E., Rodrigues, F.L., Ribeiro, L., Secchi, E.R., Kessler, F., Proietti, M.C., 2019. Plastics in sea surface waters around the Antarctic Peninsula. Sci. Rep. 9 https://doi.org/10.1038/s41598-019-40311-4.
Law, K.L., 2017. Plastics in the marine environment. Annu. Rev. Mar. Sci. https://doi.org/10.1146/annurev-marine-010816-060409.
Lusher, A.L., Munno, K., Hermabessiere, L., Carr, S., 2020. Isolation and extraction of microplastics from environmental samples: an evaluation of practical approaches and recommendations for further harmonization. Appl. Spectrosc. 74, 1049–1065. https://doi.org/10.1177/0003702820938993.
Manno, C., Fielding, S., Stowasser, G., Murphy, E.J., Thorpe, S.E., Tarling, G.A., 2020. Continuous moulting by Antarctic krill drives major pulses of carbon export in the north Scotia Sea, Southern Ocean. Nat. Commun. 11 https://doi.org/10.1038/s41467-020-19956-7.
Matano, R.P., Combes, V., Young, E.F., Meredith, M.P., 2020. Modeling the impact of ocean circulation on chlorophyll blooms around South Georgia, Southern Ocean. J. Geophys. Res. Oceans 125, 1–18. https://doi.org/10.1029/2020JC016391.
Michida, Y., et al., 2019. Guidelines for Harmonizing Ocean Surface Microplastic Monitoring Methods. Version 1.0. Ministry of the Environment, Chiyoda-ku, Japan. https://doi.org/10.25607/OBP-513, 68 pp.
Mountford, A.S., Morales Maqueda, M.A., 2021. Modeling the accumulation and transport of microplastics by sea ice. J. Geophys. Res. Oceans 126, e2020JC016826. https://doi.org/10.1029/2020JC016826.
Munari, C., Infantini, V., Scoponi, M., Rastelli, E., Corinaldesi, C., Mistri, M., 2017. Microplastics in the sediments of Terra Nova Bay (Ross Sea, Antarctica). Mar. Pollut. Bull. 122, 161–165. https://doi.org/10.1016/J.MARPOLBUL.2017.06.039.
Munno, K., de Frond, H., O'donnell, B., Rochman, C.M., 2020. Increasing the accessibility for characterizing microplastics: introducing new application-based and spectral libraries of plastic particles (SLoPP and SLoPP-E). Anal. Chem. 92, 2443–2451. https://doi.org/10.1021/ACS.ANALCHEM.9B03626/SUPPL_FILE/AC9B03626_SI_001.PDF.
Ojala, A.E.K., Kosonen, E., Weckström, J., Korkonen, S., Korhola, A., 2013. Seasonal formation of clastic-biogenic varves: the potential for palaeoenvironmental interpretations, 135, 237–247. https://doi.org/10.1080/11035897.2013.801925.
Orsi, A.H., Whitworth, T., Nowlin, W.D., 1995. On the meridional extent and fronts of the Antarctic circumpolar current. Deep-Sea Res. I 42, 641–673. https://doi.org/10.1016/0967-0637(95)00021-W.
Pohl, F., Eggenhuisen, J.T., Kane, I.A., Clare, M.A., 2020. Transport and burial of microplastics in deep-marine sediments by turbidity currents. Environ. Sci. Technol. 54 (7), 4180–4189. https://doi.org/10.1021/acs.est.9b07527.
Porter, A., Lyons, B.P., Galloway, T.S., Lewis, C., 2018. Role of marine snows in microplastic fate and bioavailability. Environ. Sci. Technol. 52, 7111–7119. https://doi.org/10.1021/acs.est.8b01000.
Poulain, M., Mercier, M.J., Brach, L., Martignac, M., Routaboul, C., Perez, E., Desjean, M. C., ter Halle, A., 2019. Small microplastics as a main contributor to plastic mass balance in the North Atlantic subtropical gyre. Environ. Sci. Technol. 53, 1157–1164. https://doi.org/10.1021/acs.est.8b05458.
Reed, S., Clark, M., Thompson, R., Hughes, K.A., 2018. Microplastics in marine sediments near Rothera Research Station, Antarctica. Mar. Pollut. Bull. 133, 460–463. https://doi.org/10.1016/j.marpolbul.2018.05.068.
Reineccius, J., Appelt, J.S., Hinrichs, T., Kaiser, D., Stern, J., Prien, R.D., Waniek, J.J., 2020. Abundance and characteristics of microfibers detected in sediment trap material from the deep subtropical North Atlantic Ocean. Sci. Total Environ. 738 https://doi.org/10.1016/j.scitotenv.2020.140354.
Reineccius, J., Waniek, J.J., 2022. First long-term evidence of microplastic pollution in the deep subtropical Northeast Atlantic. Environ. Pollut. 305 https://doi.org/10.1016/j.envpol.2022.119302.
Reisser, J., Slat, B., Noble, K., du Plessis, K., Epp, M., Proietti, M., de Sonneville, J., Becker, T., Pattiaratchi, C., 2015. The vertical distribution of buoyant plastics at sea: an observational study in the North Atlantic Gyre. Biogeosciences 12, 1249–1256. https://doi.org/10.5194/bg-12-1249-2015.
Ross, P.S., Chastain, S., Vassilenko, E., Etemadifar, A., Zimmermann, S., Quesnel, S.A., Eert, J., Solomon, E., Patankar, S., Posacka, A.M., Williams, B., 2021. Pervasive distribution of polyester fibres in the Arctic Ocean is driven by Atlantic inputs. Nat. Commun. 12 (1), 1–9. https://doi.org/10.1038/s41467-020-20347-1.
Saarni, S., Hartikainen, S., Meronen, S., Uurasjärvi, E., Kalliokoski, M., Koistinen, A., 2021. Sediment trapping – an attempt to monitor temporal variation of microplastic flux rates in aquatic systems. Environ. Pollut. 274 https://doi.org/10.1016/j.envpol.2021.116568.
van Sebille, E., Wilcox, C., Lebreton, L., Maximenko, N., Hardesty, B.D., van Franeker, J. A., Eriksen, M., Siegel, D., Galgani, F., Law, K.L., 2015. A global inventory of small floating plastic debris. Environ. Res. Lett. 10, 124006 https://doi.org/10.1088/1748-9326/10/12/124006.
Serra, T., Colomer, J., 2023. Scavenging of polystyrene microplastics by sediment particles in both turbulent and calm aquatic environments. Sci. Total Environ. 884 (April), 163720 https://doi.org/10.1016/j.scitotenv.2023.163720.
Sfriso, A.A., Tomio, Y., Rosso, B., Gambaro, A., Sfriso, A., Corami, F., Rastelli, E., Corinaldesi, C., Mistri, M., Munari, C., 2020. Microplastic accumulation in benthic invertebrates in Terra Nova Bay (Ross Sea, Antarctica). Environ. Int. 137, 105587 https://doi.org/10.1016/j.envint.2020.105587.
Simon, M., van Alst, N., Vollertsen, J., 2018. Quantification of microplastic mass and removal rates at wastewater treatment plants applying Focal Plane Array (FPA)-based Fourier Transform Infrared (FT-IR) imaging. Water Res. 142, 1–9. https://doi.org/10.1016/J.WATRES.2018.05.019.
Smetacek, V., Nicol, S., 2005. Polar Ocean Ecosystems in a Changing World, Nature. Nature Publishing Group. https://doi.org/10.1038/nature04161.
Soroldoni, S., Abreu, F., Castro, Í.B., Duarte, F.A., Pinho, G.L.L., 2017. Are antifouling paint particles a continuous source of toxic chemicals to the marine environment? J. Hazard. Mater. 330, 76–82. https://doi.org/10.1016/j.jhazmat.2017.02.001.
Suaria, G., Achtypi, A., Perold, V., Lee, J.R., Pierucci, A., Bornman, T., Aliani, S., Ryan, P., 2020a. Microplastic in oceanic surface waters: a global characterization. Sci. Adv. 6, 8493. https://doi.org/10.1126/sciadv.aay8493.
Suaria, G., Perold, V., Lee, J.R., Lebouard, F., Aliani, S., Ryan, P.G., 2020b. Floating macro- and microplastics around the Southern Ocean: results from the Antarctic Circumnavigation Expedition. Environ. Int. 136, 105494 https://doi.org/10.1016/J.ENVINT.2020.105494.
Vassilenko, E., Watkins, M., Chastain, S., Mertens, J., Posacka, A.M., Patankar, S., Ross, P.S., 2021. Domestic laundry and microfiber pollution: exploring fiber

shedding from consumer apparel textiles. PLoS One 16, e0250346. https://doi.org/10.1371/JOURNAL.PONE.0250346.

Waller, C.L., Griffiths, H.J., Waluda, C.M., Thorpe, S.E., Loaiza, I., Moreno, B., Pacherres, C.O., Hughes, K.A., 2017. Microplastics in the Antarctic marine system: an emerging area of research. Sci. Total Environ. 598, 220–227. https://doi.org/10.1016/J.SCITOTENV.2017.03.283.

Ward, P., Atkinson, A., Venables, H.J., Tarling, G.A., Whitehouse, M.J., Fielding, S., Collins, M.A., Korb, R., Black, A., Stowasser, G., Schmidt, K., Thorpe, S.E., Enderlein, P., 2012. Food web structure and bioregions in the Scotia Sea: a seasonal synthesis. Deep-Sea Res. II Top. Stud. Oceanogr. 59–60, 253–266. https://doi.org/10.1016/J.DSR2.2011.08.005.

Weiss, L., Ludwig, W., Heussner, S., Canals, M., Ghiglione, J.F., Estournel, C., Constant, M., Kerhervé, P., 2021. The missing ocean plastic sink: gone with the rivers. Science 373 (6550), 107–111. https://doi.org/10.1126/science.abe0290. Jul 2. (PMID: 34210886).

Wichmann, D., Delandmeter, P., van Sebille, E., 2019. Influence of near-surface currents on the global dispersal of marine microplastic. J. Geophys. Res. Oceans 124, 6086–6096. https://doi.org/10.1029/2019JC015328.

Wilkie Johnston, L., Bergami, E., Rowlands, E., Manno, C., 2023. Organic or junk food? Microplastic contamination in Antarctic krill and salps. R. Soc. Open Sci. 10, 221421 https://doi.org/10.1098/rsos.221421.